

Geometric properties of the Fortuin-Kasteleyn representation of the Ising model

Pengcheng Hou,¹ Sheng Fang,¹ Junfeng Wang,^{2,*} Hao Hu,^{3,†} and Youjin Deng^{1,4,‡}

¹*Hefei National Laboratory for Physical Sciences at Microscale and Department of Modern Physics, University of Science and Technology of China, Hefei, Anhui 230026, China*

²*School of Electronic Science and Applied Physics, Hefei University of Technology, Hefei, Anhui 230009, China*

³*School of Physics and Materials Science, Anhui University, Hefei, Anhui 230601, China*

⁴*CAS Center for Excellence and Synergetic Innovation Center in Quantum Information and Quantum Physics, University of Science and Technology of China, Hefei, Anhui 230026, China*



(Received 9 November 2018; revised manuscript received 26 February 2019; published 30 April 2019)

We present a Monte Carlo study of the geometric properties of Fortuin-Kasteleyn (FK) clusters of the Ising model on square [two-dimensional (2D)] and simple-cubic [three-dimensional (3D)] lattices. The wrapping probability, a dimensionless quantity characterizing the topology of the FK clusters on a torus, is found to suffer from smaller finite-size corrections than the well-known Binder ratio and yields a high-precision critical coupling as $K_c(3D) = 0.221\,654\,631(8)$. We then study other geometric properties of FK clusters at criticality. It is demonstrated that the distribution of the critical largest-cluster size C_1 follows a single-variable function as $P(C_1, L) dC_1 = \tilde{P}(x) dx$ with $x \equiv C_1/L^{d_F}$ (L is the linear size), where the fractal dimension d_F is identical to the magnetic exponent. An interesting bimodal feature is observed in distribution $\tilde{P}(x)$ in three dimensions, and attributed to the different approaching behaviors for $K \rightarrow K_c + 0^\pm$. To characterize the compactness of the FK clusters, we measure their graph distances and determine the shortest-path exponents as $d_{\min}(3D) = 1.259\,36(12)$ and $d_{\min}(2D) = 1.094\,0(2)$. Further, by excluding all the bridges from the occupied bonds, we obtain bridge-free configurations and determine the backbone exponents as $d_B(3D) = 2.167\,3(15)$ and $d_B(2D) = 1.732\,1(4)$. The estimates of the universal wrapping probabilities for the 3D Ising model and of the geometric critical exponents d_{\min} and d_B either improve over the existing results or have not been reported yet. We believe that these numerical results would provide a testing ground in the development of further theoretical treatments of the 3D Ising model.

DOI: [10.1103/PhysRevE.99.042150](https://doi.org/10.1103/PhysRevE.99.042150)

I. INTRODUCTION

The Ising model [1] plays an important role in the study of phase transitions and critical phenomena. The model exhibits a finite-temperature phase transition in two and higher dimensions. It can be solved exactly for a few two-dimensional (2D) lattices [2,3], leading to exact values of phase transition points and critical exponents, which are very often used as benchmarks for new theories and methods. In three dimensions, since an exact solution of the Ising model is still unavailable, one usually applies approximation methods or numerical simulations, among which the Monte Carlo (MC) method is probably one of the best [4,5].

Recently, the study of conformal field theories (CFTs) in three dimensions has led to significant progresses via two complementary approaches, i.e., the conformal bootstrap method [6–8] and the logarithmic conformal field theory (LCFT) [9–11]. Using the constraints of unitarity, the conformal bootstrap program has dramatically improved the precision of critical exponents for local operators in the three-dimensional (3D) Ising model [6,7]. These exponents describe the critical scaling behavior of thermodynamic quantities, including magnetization, susceptibility, energy, and heat

capacity. Intensive efforts are being carried out to treat nonunitary cases like 3D percolation [8], in which nonlocal observables are defined in terms of cluster connectivities. In the framework of LCFT, these nonlocal lattice observables are described by limits of local fields. A variety of exact structural properties can be obtained in the Fortuin-Kasteleyn (FK) representation of the q -state Potts model [9–11], referred to as the random-cluster (RC) model. The $q = 2$ and $q \rightarrow 1$ cases correspond to the Ising model and percolation, respectively.

For a given lattice \mathcal{L} , the reduced Hamiltonian of the q -state Potts model reads $\mathcal{H} = -J \sum_{\langle ij \rangle} \delta_{\sigma_i, \sigma_j}$, where each lattice site i has a spin σ_i , taking one of the q states $\sigma_i = 1, 2, \dots, q$. The summation $\langle ij \rangle$ is over all the pairs of nearest-neighbor sites and J is the interaction constant. For the Ising case, the Hamiltonian usually takes the form $\mathcal{H} = -K \sum_{\langle ij \rangle} s_i s_j$ with $s_i = \pm 1$, and thus $J = 2K$. Under the FK transformation, the partition function of the q -state Potts model can be rewritten as the RC model [12,13],

$$\mathcal{Z}_{\text{RC}}(q, v) = \sum_{\mathcal{A} \subseteq \mathcal{L}} v^{N_{\text{bond}}} q^{N_c} \quad (v = e^J - 1), \quad (1)$$

where the summation is over all subgraphs \mathcal{A} of lattice \mathcal{L} , and N_{bond} and N_c represent the number of occupied bonds and of connected components (FK clusters), respectively.

The RC model, in which $q \geq 0$ can take any real value, is itself a basic model in statistical physics and probability theory. It has yielded a host of exact results for the q -state Potts model in two dimensions [14], plays an important

*wangjf@hfut.edu.cn

†huhao@ahu.edu.cn

‡yjdeng@ustc.edu.cn

role in the development of CFT and of stochastic Loewner evolution (SLE) theory [15], and starts to shed new insights in higher dimensions in the context of LCFT [9–11]. The FK representation is also a key ingredient of the well-known Chayes-Machta-Swendsen-Wang cluster algorithm [16–18], in which nonlocal updates make the algorithm significantly suppress the so-called critical slowing down.

This paper conducts a Monte Carlo study of the FK clusters of the Ising model on square and simple-cubic lattices. We first consider the wrapping probability R , defined as the probability that at least one cluster connects to itself by wrapping around the periodic boundaries of a finite lattice of side length L , i.e., a torus. In the disordered phase $v < v_c$, the FK clusters are small and have trivial topology (contractable to a point), and $R(v < v_c)|_{L \rightarrow \infty} = 0$. In the ordered phase $v > v_c$, a giant cluster emerges and $R(v > v_c)|_{L \rightarrow \infty} = 1$. Right at criticality v_c , $R(v = v_c)|_{L \rightarrow \infty}$ approaches a universal value in between. Taking into account how such wrappings occur, we further define a family of wrapping probabilities to characterize the topology of the FK clusters on the torus. The exact values of critical wrapping probabilities have been derived for the 2D RC model [19,20]. The wrapping probability was sometimes called the crossing probability [19]. Nevertheless, the latter is now commonly used for open or fixed boundary conditions to specify the probability that a boundary segment is connected to another boundary segment [21]. In addition, the so-called spanning probability was also studied [22].

As the Binder ratio [23], the wrapping probabilities prove to be very useful in determining the critical frontier $v_c(q)$ [24–26] and in studying ensemble-dependent finite-size scaling [27,28]. Recently Jacobsen and Scullard defined the critical polynomial for the 2D RC model as $P_L \equiv R_{2d} - qR_{0d}$ [29,30], where R_{2d} corresponds to the wrapping probability in both periodic directions and R_{0d} is the probability that no wrapping exists. It is found that the solution v_L of $P_L(q, v) = 0$ converges quickly to v_c as $L \rightarrow \infty$, leading to unparalleled precision, up to $O(10^{-13})$, in the estimates of $v_c(q)$ for various lattices. Moreover, in exactly solvable cases there is no finite-size dependence at all. In three dimensions no such critical polynomial has been identified yet. Nevertheless, it is observed that for 3D percolation, some wrapping probabilities suffer from much smaller corrections than the Binder ratios, yielding rather accurate thresholds for a variety of lattices [25,26].

By performing finite-size scaling (FSS) analysis of the wrapping probabilities, we obtain a high-precision estimate of the critical coupling for the 3D Ising model as $K_c = 0.221\,654\,631(8)$. This provides an independent check of the most recent result $K_c = 0.221\,654\,626(5)$ [5], in which a state-of-the-art method, making use of cross correlations, is applied to reduce statistical errors and extensive simulations were carried out up to an impressive linear size $L = 1024$. The universal values of the wrapping probabilities for the 3D Ising model are numerically determined.

We then study other geometric properties of the FK clusters of the Ising model at criticality. The probability distribution of the largest-cluster size C_1 is demonstrated to follow a single-variable function as $P(C_1, L) dC_1 = \tilde{P}(x) dx$ with $x \equiv C_1/L^{d_F}$, where, as expected, the fractal dimension d_F is identical to the magnetic renormalization exponent y_h . The function

$\tilde{P}(x)$ displays a clear bimodal feature in three dimensions, while in two dimensions, it exhibits an asymmetric peak with a shoulder shape at the smaller- x side. By fine-tuning simulations at L -dependent coupling $K \rightarrow K_c + 0^\pm$, we find that the two modes correspond to the distinct asymptotic behaviors approaching from the low- and high-temperature sides. For the full FK configuration, we measure the cluster number per site $n(s, L)$ of size s and demonstrate that the standard scaling $n(s, L) \sim s^{-\tau} \tilde{n}(s/L^{d_F})$ is obeyed both in two and three dimensions, and the hyperscaling relation $\tau = 1 + d/d_F$ is well satisfied (d is the spatial dimension). To characterize the compactness of the FK clusters, we record their graph distances and determine the shortest-path exponents as $d_{\min}(3D) = 1.259\,36(12)$ and $d_{\min}(2D) = 1.094\,0(2)$. In addition, we classify the occupied bonds into bridges and nonbridges; an occupied bond is a bridge *iff* its deletion leads to the breaking of a FK cluster. By excluding all the bridges, we obtain bridge-free configurations and determine the backbone exponents as $d_B(3D) = 2.167\,3(15)$ and $d_B(2D) = 1.732\,1(4)$. These estimates of d_{\min} and d_B either improve over the existing results or have not been reported yet, to our knowledge.

The remainder of this paper is organized as follows. Section II describes the simulation and sampled quantities. Section III presents results for the wrapping probabilities of FK clusters and the estimate of the critical coupling K_c for the 3D Ising model. Section IV studies other geometric properties of the FK clusters, including the probability distribution of the largest-cluster size, the cluster number per site $n(s, L)$, the graph distances of the FK clusters, the size of the largest cluster in the bridge-free configuration, and the thermodynamic bond densities of various types. A brief summary and discussion is given in Sec. V. The Appendix collects results on other observables.

II. SIMULATION AND SAMPLED QUANTITIES

We employ the Wolff cluster flipping algorithm [31] and the Swendsen-Wang algorithm [16]. The latter is mainly used to generate FK clusters over the whole lattice. The occupied bonds on a FK configuration are classified into bridges and nonbridges [32,33]. A bridge bond is an occupied bond whose deletion would break a cluster. All bridges are deleted by the procedure in Refs. [32,33]. In a bridge-free configuration, any pairs of two sites are either disconnected or connected by at least two independent paths of nonbridges, which form the backbone of the FK configuration. Our simulation in three dimensions is up to $L = 512$. For $L = 512, 384, 256$, and 192 , the numbers of samples are about 4×10^6 , 1.5×10^7 , 1.3×10^8 , and 1.3×10^8 , respectively. For each $L \leq 128$, no less than 5×10^8 samples are generated. The 2D simulation is up to $L = 1024$. The numbers of samples are about 3.6×10^6 and 10^7 for $L = 1024$ and 768 , respectively, no less than 2×10^7 samples for $L = 512, 384, 256, 192, 128$, and 96 , and around 10^8 for each $L \leq 64$. Given a FK configuration, we sample the following observables:

- (a) The indicators $\mathcal{R}^{(x)}$, $\mathcal{R}^{(y)}$, and $\mathcal{R}^{(z)}$. We set $\mathcal{R}^{(x)} = 1$ to record the event that at least one cluster wraps around the lattice in the x direction and otherwise $\mathcal{R}^{(x)} = 0$.
- (b) The size of the largest cluster \mathcal{C}_1 .

(c) The size of the largest cluster on the bridge-free configuration $\mathcal{C}_{1,\text{bf}}$.

(d) An observable $\mathcal{S} := \max_C \max_{y \in C} d(x_C, y)$ is used to determine the shortest-path exponent. Here $d(x, y)$ denotes the graph distance from vertex x to vertex y , and x_C is the vertex in cluster C with the smallest vertex label, according to some fixed (but arbitrary) vertex labeling.

(e) The numbers \mathcal{N}_b , \mathcal{N}_j , \mathcal{N}_n of branch, junction, and nonbridge bonds, respectively. The bridge bond is a junction bond if neither of the two resulting clusters is a tree; otherwise, it is a branch bond [32,33].

(f) The square \mathcal{M}^2 and the fourth power \mathcal{M}^4 of the magnetization density \mathcal{M} , where \mathcal{M} is defined as $\mathcal{M} = \frac{1}{L^d} \sum_i s_i$ with d the spatial dimension.

From these observables we calculate the following quantities:

(a) The wrapping probabilities

$$\begin{aligned} R^{(x)} &= \langle \mathcal{R}^{(x)} \rangle = \langle \mathcal{R}^{(y)} \rangle = \langle \mathcal{R}^{(z)} \rangle, \\ R^{(2)} &= \langle \mathcal{R}^{(x)} \mathcal{R}^{(y)} \rangle = \langle \mathcal{R}^{(x)} \mathcal{R}^{(z)} \rangle = \langle \mathcal{R}^{(y)} \mathcal{R}^{(z)} \rangle, \\ R^{(3)} &= \langle \mathcal{R}^{(x)} \mathcal{R}^{(y)} \mathcal{R}^{(z)} \rangle, \end{aligned} \quad (2)$$

where $\langle \cdot \rangle$ means statistical average. Here $R^{(x)}$, $R^{(2)}$, and $R^{(3)}$ give the probabilities that a winding exists in the x direction, in two of the three possible directions, and simultaneously in the three directions, respectively. At K_c , these wrapping probabilities take nonzero universal values in the thermodynamic limit $L \rightarrow \infty$.

(b) The mean size of the largest cluster $C_1 = \langle \mathcal{C}_1 \rangle$, which scales as $C_1 \sim L^{d_f}$ at K_c , with d_f the fractal dimension of the FK clusters.

(c) The mean size of the largest cluster in bridge-free configurations $\mathcal{C}_{1,\text{bf}} = \langle \mathcal{C}_{1,\text{bf}} \rangle$. It scales as $\mathcal{C}_{1,\text{bf}} \sim L^{d_b}$ at K_c , with d_b the backbone fractal dimension [32,33]. The exponent d_b used to be calculated from the subset of the incipient infinite cluster sites carrying the current when a voltage difference is applied between two sites far apart [34,35].

(d) The mean shortest-path distance $S = \langle \mathcal{S} \rangle$, which scales as $S \sim L^{d_{\min}}$ at K_c , with d_{\min} the shortest-path fractal dimension.

(e) The number densities $\rho_b = \langle \mathcal{N}_b \rangle / L^d$, $\rho_j = \langle \mathcal{N}_j \rangle / V$ and $\rho_n = \langle \mathcal{N}_n \rangle / V$ of the branch, junction and nonbridge bonds, respectively. The leading scaling terms of these bond densities are proportional to $L^{y_i - d}$.

(f) The Binder cumulant

$$Q_m = \frac{\langle \mathcal{M}^4 \rangle}{\langle \mathcal{M}^2 \rangle^2}. \quad (3)$$

In addition, we record the statistics of the cluster number per site $n(s, L)$ of size s and the probability distribution $P(C_1, L) dC_1$ for the largest-cluster size C_1 .

For computational efficiency, we use the standard reweighting method [36] to obtain the expectations of the wrapping probabilities and the Binder cumulant for multiple values of K around K_c .

III. WRAPPING PROBABILITIES AND CRITICAL POINT IN THREE DIMENSIONS

In numerical studies of phase transitions, dimensionless quantities like the Binder cumulant Q_m are known to pro-

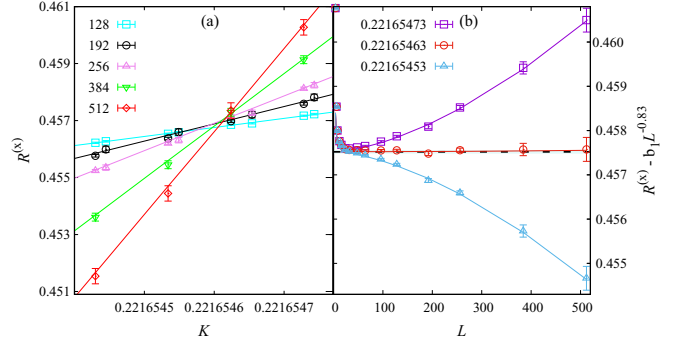


FIG. 1. Plots of $R^{(x)}$ vs K for different system sizes L (a) and $R^{(x)}(K, L) - b_1 L^{-0.83}$ vs L for fixed values of K (b) for the 3D Ising model. The value of $b_1 = -0.0393$ is taken from Table I.

vide powerful tools for locating critical points. The wrapping probabilities, being topological and dimensionless quantities, should also provide a useful method for estimating K_c . This is demonstrated in Fig. 1(a) for the 3D Ising model. The intersections of the $R^{(x)}$ data for different system sizes L would give the critical couplings $K_c \approx 0.2216546$, with an uncertainty at the seventh decimal place.

In order to estimate K_c more accurately, we resort to the fitting of the data. Around K_c , we perform least-squares fits of the MC data for the wrapping probabilities $R^{(x)}$, $R^{(2)}$, $R^{(3)}$ and the Binder cumulant Q_m by the ansatz

$$\begin{aligned} \mathcal{O}(\epsilon, L) &= \mathcal{O}_c + \sum_{k=1}^2 q_k \epsilon^k L^{ky_i} + c_1 \epsilon L^{y_i + y_j} \\ &\quad + b_1 L^{y_i} + b_2 L^{-2} + b_3 L^{-3}, \end{aligned} \quad (4)$$

where $\epsilon = K_c - K$, \mathcal{O}_c is a universal constant, y_i is the thermal scaling exponent and y_j is the leading correction exponent.

As a precaution against correction-to-scaling terms that we have neglected in our chosen ansatz, we impose a lower cutoff $L \geq L_{\min}$ on the data points admitted in the fit and systematically study the effect on the χ^2 value when L_{\min} is increased. In general, our preferred fit for any given ansatz corresponds to the smallest L_{\min} for which χ^2 divided by the number of degrees of freedom (DFs) is $O(1)$, and for which subsequent increases in L_{\min} do not cause χ^2 to drop by much more than one unit per degree of freedom. In the fits with y_i free and $b_3 = 0$ fixed, our results of y_i estimated from $R^{(x)}$ are consistent with $y_i \approx -0.83$, as determined elsewhere [37,38]. In the subsequent fits, we fix $y_i = -0.83$ for all quantities since in theory y_i should be a universal correction exponent. In most cases, when performing the fits with y_i fixed, we include the correction term $b_3 L^{-3}$. Nevertheless, we observe that the $R^{(x)}(L)$ values exhibit smaller finite-size corrections, which can be sufficiently described by term $b_1 L^{-0.83} + b_2 L^{-2}$; when b_3 is set to be a free parameter, the estimated error margin of b_3 is bigger than the magnitude of b_3 itself. Table I summarizes the fitting results.

From Table I we observe that in comparison with Q_m , the wrapping probabilities, especially $R^{(x)}$, clearly have smaller amplitudes of the leading corrections. Due to the weaker corrections, the results of K_c fitted from the wrapping

TABLE I. Fits of the wrapping probabilities $R^{(x)}$, $R^{(2)}$, $R^{(3)}$ and the Binder cumulant Q_m for the 3D Ising model. ‘‘Obs.’’ is the abbreviation of ‘‘observables.’’

Obs.	L_{\min}	χ^2/DFs	K_c	y_t	\mathcal{O}_c	q_1	b_1	y_i	b_2	b_3
$R^{(x)}$	12	86.1/156	0.221 654 633(3)	1.60(2)	0.457 59(4)	-1.4(1)	-0.036(2)	-0.80(2)	0.009(9)	-
	16	75.7/140	0.221 654 631(4)	1.59(2)	0.457 53(6)	-1.4(1)	-0.040(5)	-0.84(4)	0.04(3)	-
	24	71.5/124	0.221 654 629(4)	1.59(2)	0.457 49(9)	-1.4(2)	-0.05(2)	-0.88(8)	0.08(8)	-
	12	89.4/157	0.221 654 629(2)	1.60(2)	0.457 529(7)	-1.38(10)	-0.038 9(2)	-0.83	0.024(2)	-
	16	75.8/141	0.221 654 631(2)	1.59(2)	0.457 54(1)	-1.4(2)	-0.039 3(3)	-0.83	0.032(4)	-
$R^{(2)}$	24	72.0/125	0.221 654 631(3)	1.59(2)	0.457 55(2)	-1.4(2)	-0.039 4(5)	-0.83	0.03(2)	-
	12	91.9/134	0.221 654 633(3)	1.60(2)	0.332 01(4)	-1.3(1)	-0.093(3)	-0.874(9)	-0.25(1)	-
	16	73.8/121	0.221 654 629(4)	1.59(2)	0.331 93(6)	-1.4(1)	-0.101(6)	-0.90(2)	-0.21(3)	-
	24	71.2/108	0.221 654 628(4)	1.59(2)	0.331 90(9)	-1.4(2)	-0.11(2)	-0.92(4)	-0.17(9)	-
	12	98.6/134	0.221 654 637(3)	1.60(2)	0.332 12(2)	-1.3(1)	-0.080 3(5)	-0.83	-0.37(2)	0.45(11)
$R^{(3)}$	16	75.9/121	0.221 654 633(3)	1.59(2)	0.332 07(3)	-1.4(2)	-0.078(1)	-0.83	-0.47(5)	1.5(4)
	24	72.1/108	0.221 654 631(4)	1.59(2)	0.332 04(4)	-1.4(2)	-0.076(2)	-0.83	-0.6(2)	3(2)
	12	110.4/134	0.221 654 634(3)	1.60(2)	0.267 25(4)	-1.3(1)	-0.117(3)	-0.885(8)	-0.32(2)	-
	16	87.9/121	0.221 654 629(4)	1.59(2)	0.267 14(5)	-1.3(1)	-0.131(7)	-0.92(2)	-0.25(3)	-
	24	85.9/108	0.221 654 629(5)	1.59(2)	0.267 13(9)	-1.3(2)	-0.13(2)	-0.92(4)	-0.24(9)	-
Q_m	16	86.0/135	0.221 654 635(3)	1.59(2)	0.267 34(3)	-1.3(2)	-0.094(1)	-0.83	-0.66(5)	2.3(4)
	24	80.1/122	0.221 654 633(4)	1.59(2)	0.267 30(4)	-1.3(2)	-0.092(2)	-0.83	-0.8(2)	4(2)
	32	76.6/109	0.221 654 628(5)	1.58(2)	0.267 19(8)	-1.4(2)	-0.085(5)	-0.83	-1.5(5)	16(8)
	12	83.3/135	0.221 654 623(4)	1.59(2)	1.603 53(8)	2.1(2)	-0.271(5)	-0.860(7)	-0.25(3)	-
	16	80.9/122	0.221 654 624(5)	1.59(2)	1.603 5(2)	2.1(3)	-0.276(10)	-0.87(2)	-0.22(6)	-
Q_m	24	77.5/109	0.221 654 623(6)	1.59(2)	1.603 6(2)	2.1(3)	-0.27(3)	-0.85(3)	-0.3(2)	-
	12	86.0/135	0.221 654 617(3)	1.59(2)	1.603 76(3)	2.1(3)	-0.245(1)	-0.83	-0.55(2)	1.0(3)
	16	80.1/122	0.221 654 621(4)	1.59(2)	1.603 68(5)	2.1(3)	-0.241(2)	-0.83	-0.49(4)	2.5(8)
	24	76.6/109	0.221 654 622(5)	1.59(2)	1.603 65(8)	2.1(3)	-0.239(4)	-0.83	-0.65(9)	4(3)

probabilities have relatively smaller error bars. The estimates of K_c from Q_m are systematically smaller than those from the wrapping probabilities, despite that they agree with each other within the combined error bar. Note that the fitting formula is unavoidably approximate. For instance, it does not include finite-size corrections originated from the regular part of the free energy. These corrections should exist in the Q_m data but are absent in the wrapping probabilities, which are nonlocal quantities. We regard that the fitting results from the wrapping probabilities, especially $R^{(x)}$, are more reliable. Table I also gives the estimate of the thermal exponent $y_t \approx 1.59$.

After comparing the fitting results of K_c from various wrapping probabilities, we present our final estimate as $K_c(3D) = 0.221\ 654\ 631(8)$, where the finally quoted error margin $\delta =$

8×10^{-9} is taken by requiring that $K_c \pm \delta$ cover almost all the fitting K_c results from the wrapping probabilities. Figure 1(b) demonstrates the values of K_c and $R^{(x)}$, where $R^{(x)} - b_1 L^{-0.83}$ is plotted versus L . The value of the parameter b_1 is taken from Table I. Precisely at $K = K_c$, the $L \rightarrow \infty$ data tend to a horizontal line, whereas the data with $K \neq K_c$ bend upward or downward.

Our estimate agrees well with the most recent result 0.221 654 626(5) by Ferrenberg *et al.* [5] within one error bar but with slightly lower precision. Since Ref. [5] used cross correlations to reduce statistical errors and carried out simulations up to an impressive linear size $L = 1024$, our result provides a valuable and independent check. A previous estimate 0.221 654 55(3) [37] reported by one of our authors and his collaborator is ruled out.

TABLE II. Fits of C_1 for the 3D and 2D Ising models.

	L_{\min}	χ^2/DF	d_F	a_0	b_1	y_1	b_2
3D	8	6.2/8	2.481 7(3)	1.107(2)	-0.096(10)	-0.78(7)	-0.30(4)
	12	6.2/7	2.481 7(4)	1.107(3)	-0.10(3)	-0.79(12)	-0.29(10)
	12	6.3/8	2.481 82(6)	1.106 0(4)	-0.106(3)	-0.83	-0.25(3)
	16	5.6/7	2.481 78(8)	1.106 3(5)	-0.109(5)	-0.83	-0.21(5)
	24	5.2/6	2.481 84(13)	1.105 9(9)	-0.104(9)	-0.83	-0.3(2)
2D	8	14.0/11	1.875 01(2)	1.007 0(1)	-0.039(7)	-1.6(1)	-
	12	14.0/10	1.875 01(3)	1.007 0(2)	-0.04(2)	-1.6(3)	-
	16	12.3/9	1.875 02(3)	1.007 0(2)	-0.12(15)	-2.0(5)	-
	16	12.3/10	1.875 024(13)	1.006 91(6)	-0.12(1)	-2	-
	24	12.2/9	1.875 020(17)	1.006 93(8)	-0.13(3)	-2	-

In Appendix 1, we determine the thermal exponent as $y_t = 1.5870(5)$ by analyzing the covariance of the wrapping probability and the energy density, which is also consistent with the result $1.5875(3)$ in Ref. [5].

IV. GEOMETRICAL PROPERTIES OF FK CLUSTERS AT K_c

Fixing K at our estimated critical coupling 0.22165463 for the simple cubic lattice and the exact solution $\ln(1 + \sqrt{2})/2 \approx 0.44068679$ for the square lattice, we analyze geometrical quantities defined in Sec. II. These include the size of the largest cluster C_1 , the shortest-path distance S , and the size of the largest cluster on the bridge-free configuration $C_{1,\text{bf}}$. These analyses allow us to estimate the fractal dimension d_F , the shortest-path fractal dimension d_{min} , and the backbone fractal dimension d_B . In addition, we study the cluster-size distribution and the probability distribution of the size of the largest cluster.

A. Fractal dimension d_F and the probability distribution of the largest-cluster size

In order to estimate d_F , we fit the MC data of C_1 to the following equation:

$$\mathcal{A} = L^{y_A}(a_0 + b_1 L^{y_1} + b_2 L^{y_2}). \quad (5)$$

For the 3D Ising model, when we perform the fit with $y_2 = -2$ fixed and y_1 free, we observe that $y_1 \approx -0.83$. To reduce one fitting parameter, in the subsequent fit we fix $y_1 = -0.83$ and $y_2 = -2$. The fitting results are shown in Table II. We also try the fit using $b_1 L^{-1} + b_2 L^{-2}$ as correction terms for both two and three dimensions, in which case b_2 cannot be determined and the corresponding results are not shown in the table.

Comparing these fits, we determine the fractal dimensions $d_F = 2.4818(4)$ for three dimensions and $1.87501(4)$ for two dimensions. The latter agrees with the exact value $y_h = 15/8$ [39,40]. In Fig. 2 we plot C_1/L^{d_F} versus $L^{-0.83}$ using three different values of d_F for the 3D Ising model: namely our estimate, as well as the estimate plus or minus three standard deviations. As L increases, the data with $d_F = 2.4806$ and $d_F = 2.4830$ bend upward and downward, respectively, while

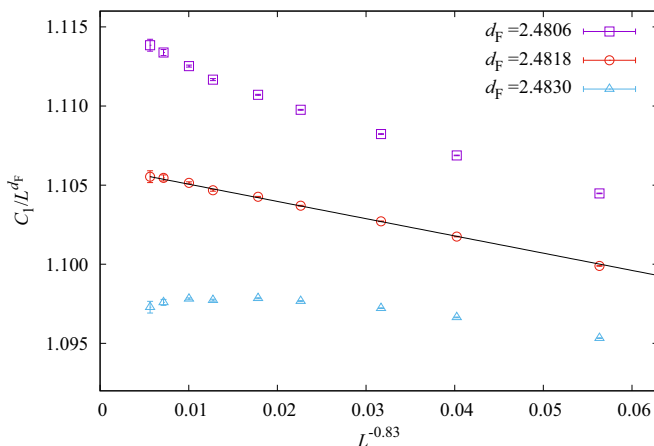


FIG. 2. Plots of C_1/L^{d_F} vs $L^{-0.83}$ for the critical 3D Ising model.

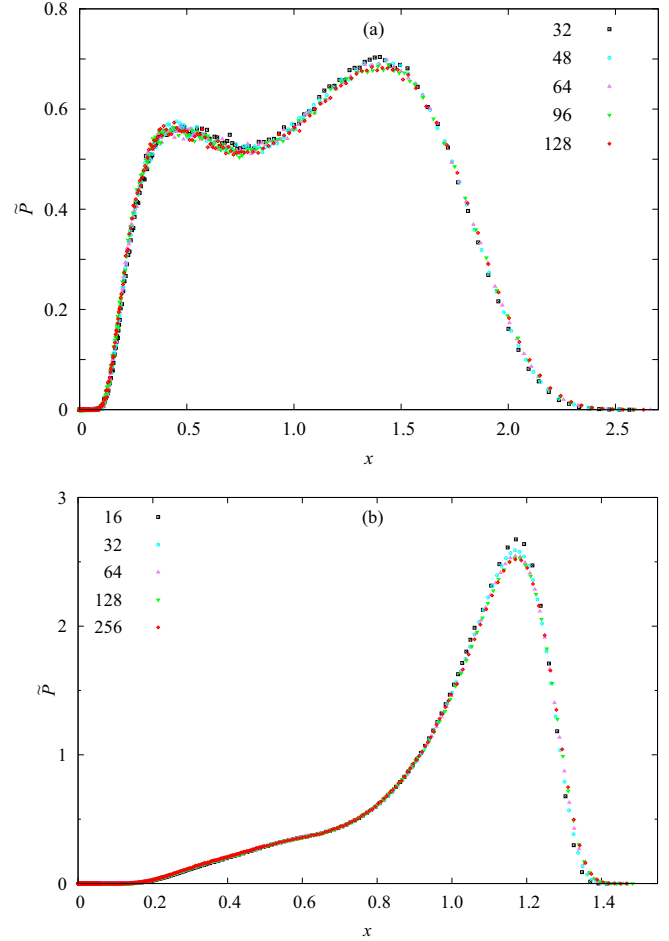


FIG. 3. Probability density distribution of the largest-cluster size for three dimensions (a) and two dimensions (b) at K_c , with $x \equiv C_1/L^{d_F}$.

the data with $d_F = 2.4818$ are consistent with a straight line. This illustrates the reliability of our estimate.

We also study the probability distribution $P(C_1, L)dC_1$ of the size of the largest cluster C_1 . In the MC simulation, $P(C_1, L)dC_1$ is measured by the fraction of the number of the configurations on which the size of the largest cluster lies between $C_1 \sim C_1 + dC_1$. According to finite-size scaling theory, we expect that $P(C_1, L)dC_1$ can be expressed as a single-variable function $\tilde{P}(x)dx$, with $x \equiv C_1/L^{d_F}$. This is well confirmed by Fig. 3, where the data for different system sizes collapse on top of each other. Interestingly, we see that the scaling function $\tilde{P}(x)$ exhibits a bimodal structure in three dimensions and a single peak with a wide shoulder shape in the small- x side in two dimensions.

To understand the bimodal structure in three dimensions, we explore $\tilde{P}(x)$ in the critical window $\Delta \equiv L^{y_t}(K - K_c)$, with Δ a finite constant. An example with $\Delta = \pm 0.1$ is shown in Fig. 4(a), where the distributions become to have a single peak with a wide shoulder shape. Therefore, it is reasonable to assume that the asymptotic peak locations $x_{\text{max}}(\Delta \rightarrow 0^\pm)$ are actually different. From the similarity between the 3D low-temperature distribution with $\Delta = 0.1$ [Fig. 4(a)] and the 2D critical one [Fig. 3(b)], we expect that a bimodal distribution would appear for two dimensions in the high-temperature

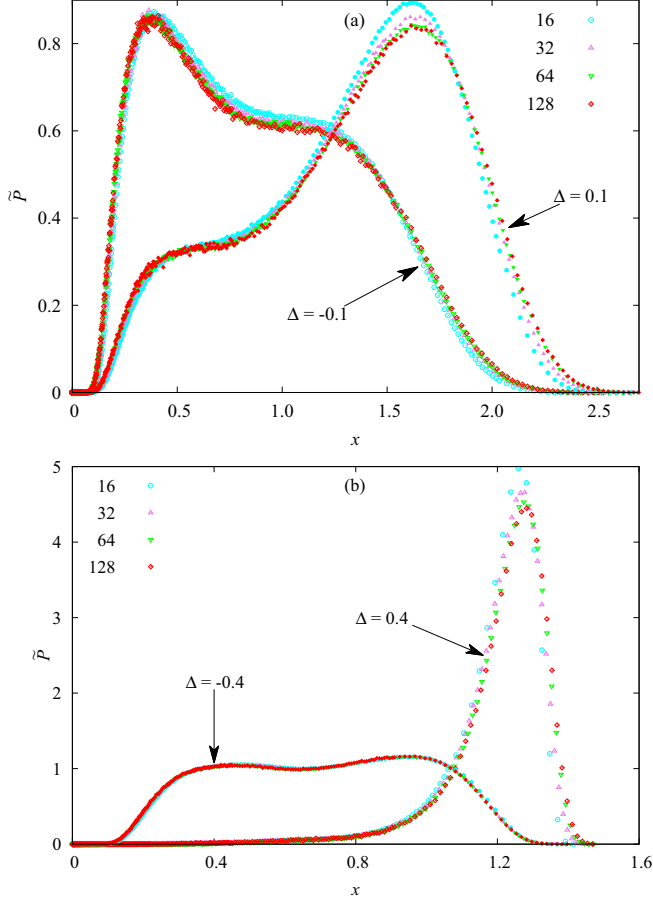


FIG. 4. Probability density distribution of the largest-cluster size for three dimensions (a) and two dimensions (b) with $K = K_c \pm \Delta L^{-y_1}$.

region with $\Delta < 0$. The 2D results with $\Delta = \pm 0.4$ are shown in Fig. 4(b), confirming our expectation.

B. Cluster-size distribution

We consider the critical cluster-number density $n(s, L)$ of size s , of which the scaling behavior is expected to follow

$$n(s, L) = s^{-\tau} \tilde{n}(s/L^{d_F}), \quad (6)$$

where $\tau = 1 + d/d_F$ is the Fisher exponent and $\tilde{n}(x)$ with $x \equiv s/L^{d_F}$ is a universal scaling function. The above scaling relation of cluster-size distribution was found to be satisfied for the Ising model in three dimensions [41,42] and two dimensions [43]. From $d_F \approx 2.4818$ (3D) or $15/8$ (2D), one has $\tau \approx 2.2088$ (3D) or $31/15$ (2D), respectively. In the main plots of Fig. 5, we show a log-log plot of $n(s)$ versus s for $L = 64, 96, 128, 192,$ and 256 for the 3D Ising model, and for $L = 128, 192,$ and 256 for the 2D Ising model. The straight lines with slope -2.2088 (3D) and $31/15$ (2D) are drawn for comparison with the MC data. In these plots, we observe clearly the power-law behaviors $n(s, \infty) \sim s^{-2.2088}$ (3D) and $n(s, \infty) \sim s^{-31/15}$ (2D), respectively. These results are more precise than previous results [41–43].

In order to display the universal scaling function $\tilde{n}(x)$, we further plot $s^{2.2088}n(s, L)$ versus $s/L^{2.4818}$ (3D) and

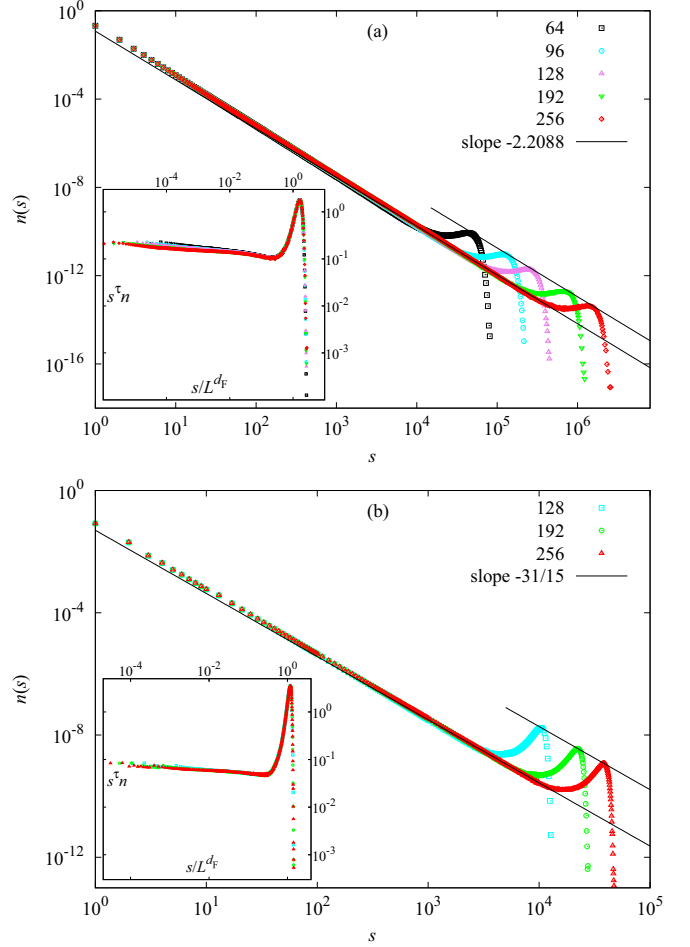


FIG. 5. Cluster-size distribution for FK clusters for three dimensions (a) and two dimensions (b) at criticality. In both cases, the insets show $s^\tau n(s)$ vs s/L^{d_F} .

$s^{31/15}n(s, L)$ versus $s/L^{15/8}$ (2D) for several system sizes, and show them in the insets of Fig. 5. We find a good collapse of those curves for different system sizes, which provides strong numerical evidence for the conjectured scaling (6).

C. Shortest-path fractal dimension d_{\min}

We estimate the shortest-path fractal dimension d_{\min} for the 3D and 2D Ising models by studying the shortest-path distance S . The MC data for S are fitted to Eq. (5) with the exponent y_A being replaced by d_{\min} . For the 3D Ising model, with $y_2 = -3$ and y_1 being free, we obtain $y_1 = -1.8(2)$, much smaller than $y_i \approx -0.83$ from the leading irrelevant scaling field. On this basis, we further perform the fit with $y_1 = -1.8$ and $y_2 = -3$ fixed. For the 2D Ising model, setting $b_2 = 0$ and y_1 free, y_1 cannot be determined by our MC data. We then try the fit with $y_1 = -2$ fixed and find b_1 consistent with zero. On this basis, we perform the fit with $b_1 = 0$ and $b_2 = 0$. Thus, S suffers rather small finite-size corrections both in two and three dimensions.

The fitting results are shown in Table III. From these fits, we estimate $d_{\min} = 1.25936(12)$ (3D) and $1.0940(2)$ (2D), respectively. As far as we know, the shortest-path fractal

TABLE III. Fits of S for the 3D and 2D Ising models.

	L_{\min}	χ^2/DF	d_{\min}	a_0	b_1	y_1	b_2
3D	16	9.3/6	1.259 34(5)	2.045 3(5)	-5.0(8)	-1.78(5)	27(5)
	24	6.2/5	1.259 42(6)	2.044 3(7)	-9(4)	-1.9(1)	60(24)
	16	9.5/7	1.259 36(2)	2.045 0(2)	-5.38(4)	-1.8	29.5(7)
	24	8.0/6	1.259 34(3)	2.045 2(3)	-5.48(9)	-1.8	33(3)
	32	7.0/5	1.259 37(4)	2.044 9(4)	-5.3(2)	-1.8	25(9)
2D	96	6.7/5	1.093 99(6)	1.334 7(5)	5(2)	-2	-
	128	2.9/4	1.094 09(8)	1.333 9(6)	10(3)	-2	-
	192	2.9/3	1.094 08(12)	1.334(1)	9(9)	-2	-
	192	4.2/4	1.093 96(5)	1.335 0(4)	-	-	-
	256	3.0/3	1.094 00(6)	1.334 7(5)	-	-	-

dimension of the 3D Ising FK clusters has not been previously estimated. The 2D result improves over the previous reported value $d_{\min} = 1.095 5(10)$ [44].

To illustrate our estimate, Fig. 6 shows a plot of $S/L^{d_{\min}}$ versus $L^{-1.8}$ (3D) and a plot of $S/L^{d_{\min}}$ versus L^{-2} (2D) at three different d_{\min} values. In both cases, using the estimated values of d_{\min} produces a straight line, but in contrast the other two curves bend upward or downward for large L . The figure suggests that the true value of d_{\min} does indeed lie within three error bars of our estimate.

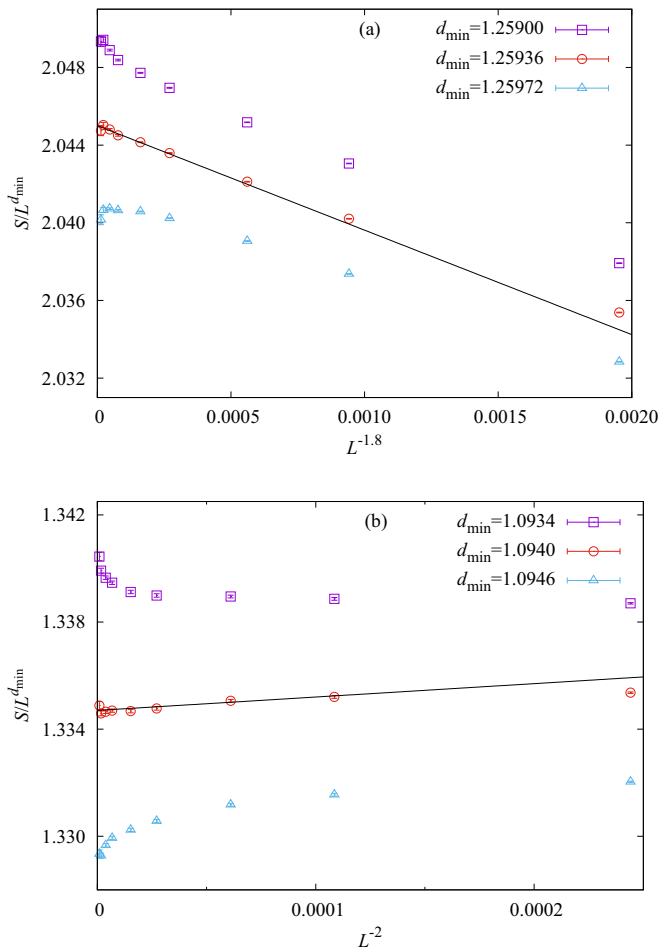


FIG. 6. Plots of $S/L^{d_{\min}}$ vs $L^{-1.8}$ or L^{-2} for the critical 3D (a) or 2D Ising model (b), respectively.

D. Backbone fractal dimension d_B

In order to estimate the backbone fractal dimension d_B for the 3D and 2D Ising models, we fit the MC data of $C_{1,\text{bf}}$ to Eq. (5) with y_A being replaced by d_B . For the 3D Ising model, in the fit with $y_2 = -2$ fixed and y_1 free, we observe that $y_1 \approx -0.83$. On this basis we fix $y_1 = -0.83$ and $y_2 = -2$. For the 2D Ising model, when set $b_2 = 0$ and leave y_1 free, we find that $y_1 \approx -0.67$, which is an unknown correction exponent

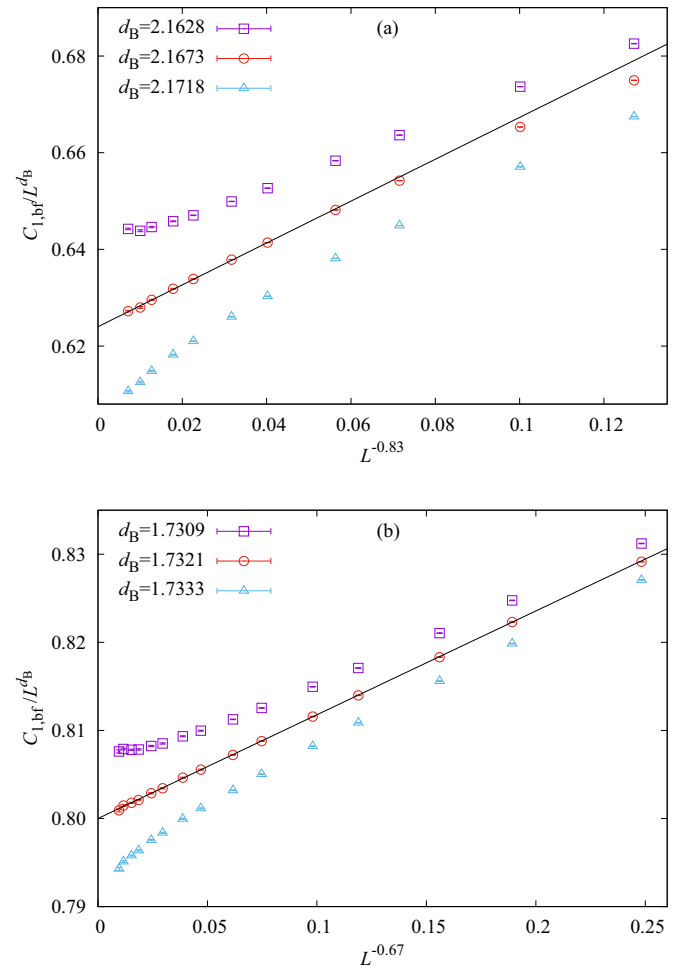


FIG. 7. Plots of $C_{1,\text{bf}}/L^{d_B}$ vs $L^{-0.83}$ or vs $L^{-0.67}$ for the critical 3D (a) or 2D (b) Ising model, respectively.

TABLE IV. Fits of $C_{1,bf}$ for the 3D and 2D Ising models.

	L_{\min}	χ^2/DF	d_B	a_0	b_1	y_1	b_2
3D	8	8.9/6	2.168 0(7)	0.621(3)	0.40(2)	-0.78(3)	-0.50(8)
	12	6.9/5	2.166 9(9)	0.626(4)	0.46(6)	-0.85(6)	-0.8(3)
	12	7.0/6	2.167 3(2)	0.624 2(8)	0.439(6)	-0.83	-0.71(5)
	16	6.0/5	2.167 1(3)	0.615(1)	0.433(9)	-0.83	-0.6(1)
	24	4.8/4	2.167 4(5)	0.624(2)	0.45(2)	-0.83	-0.9(3)
2D	8	12.7/11	1.732 14(13)	0.7997(7)	0.116 8(9)	-0.66(2)	-
	12	10.5/10	1.732 0(2)	0.8008(10)	0.119(2)	-0.69(2)	-
	16	8.6/9	1.732 2(3)	0.7996(14)	0.116(3)	-0.66(3)	-
	8	13.1/12	1.732 07(4)	0.800 1(2)	0.117 2(4)	-0.67	-
	12	11.2/11	1.732 10(4)	0.800 0(2)	0.117 8(6)	-0.67	-
	16	8.8/10	1.732 06(5)	0.800 2(3)	0.116 9(9)	-0.67	-

and suggests rather strong finite-size corrections. To reduce one fitting parameter, we perform the subsequent fit with both $y_1 = -0.67$ and $b_2 = 0$ fixed.

The fitting results are shown in Table IV. Comparing these fits, we estimate the backbone fractal dimension as $d_B = 2.167 3(15)$ (3D) and $1.732 1(4)$ (2D), respectively. The 3D result improves over the previous reported value $d_B(3D) = 2.171(4)$ [45], and the 2D result rules out the previous estimate $d_B(2D) = 1.730 4(3)$ [46]. These previous reported values were estimated by studying the scaling behavior of the probability that a pair of lattice sites at a distance r are connected by at least two mutually independent paths. Similarly, by using three different d_B values, in Fig. 7 we plot $C_{1,bf}/L^{d_B}$ versus $L^{-0.83}$ (3D) or $L^{-0.67}$ (2D), illustrating the reliability of our estimate of d_B .

E. Bond densities ρ_b , ρ_j , and ρ_n

In order to estimate the critical bond densities for branch, junction and nonbridge bonds for the 3D and 2D Ising models, we fit the MC data of ρ_b , ρ_j and ρ_n to the ansatz

$$\rho = \rho_0 + L^{y_1-d}(a + bL^{y_1}) \tag{7}$$

with $y_1 - d = -1.413$ (3D) and -1 (2D) fixed. For the 3D Ising model, in the fits with y_1 free, we observe that $y_1 \approx -1.2$ for ρ_b ; however, for ρ_j and ρ_n , we cannot obtain stable fitting results. On this basis, in the subsequent fits we fix $y_1 = -1.2$. For the 2D Ising model, the correction exponent y_1 for ρ_b , ρ_j , and ρ_n can not be determined by our MC data when leaving it free. We then try the fits with fixed $y_1 = -1$ or -2 respectively. In both cases, b_1 is found to be consistent

TABLE V. Fits of the bond densities ρ_b , ρ_j , and ρ_n for the 3D and 2D Ising models.

	L_{\min}	χ^2/DF	ρ_0	a	b	y_1
3D	ρ_b	8	0.176 526 50(5)	-0.136 9(1)	0.025(6)	-1.2(2)
		12	0.176 526 47(5)	-0.136 8(1)	0.05(4)	-1.5(3)
		16	0.176 526 49(6)	-0.136 9(2)	0.03(3)	-1.2(5)
		12	0.176 526 50(4)	-0.136 92(5)	0.028(2)	-1.2
		16	0.176 526 49(4)	-0.136 88(6)	0.026(3)	-1.2
		24	0.176 526 48(4)	-0.136 85(8)	0.023(5)	-1.2
	ρ_j	24	0.010 298 17(2)	-0.070 29(3)	0.008(2)	-1.2
		32	0.010 298 18(2)	-0.070 32(4)	0.011(4)	-1.2
		48	0.010 298 19(3)	-0.070 37(8)	0.018(9)	-1.2
		12	0.051 342 34(9)	0.340 1(1)	-0.052(4)	-1.2
		16	0.051 342 35(9)	0.340 1(2)	-0.049(6)	-1.2
		24	0.051 342 35(10)	0.340 1(2)	-0.05(1)	-1.2
2D	ρ_b	24	0.183 250 4(3)	-0.109 68(9)	0.004(3)	-1
		24	0.183 250 3(3)	-0.109 64(6)	0.09(6)	-2
		24	0.183 250 0(3)	-0.109 56(4)	-	-
		32	0.183 250 2(3)	-0.109 60(4)	-	-
		16	0.023 856 2(2)	-0.110 52(4)	-0.0001(8)	-1
		16	0.023 856 2(2)	-0.110 52(3)	0.001(9)	-2
	ρ_j	16	0.023 857 2(2)	-0.110 52(2)	-	-
		24	0.023 856 2(2)	-0.110 52(2)	-	-
		24	0.292 893 6(8)	0.311 4(2)	-0.005(6)	-1
		24	0.292 893 7(7)	0.311 4(1)	-0.1(1)	-2
		24	0.292 894 0(6)	0.311 25(7)	-	-
		32	0.292 893 7(6)	0.311 33(9)	-	-

TABLE VI. Summary of the estimates of the critical exponents and the universal critical wrapping probabilities. The value of d_F from Ref. [5] is calculated by the scaling law $d_F = (\gamma + d\nu)/2\nu$.

	2D		3D	
	Present	Previous	Present	Previous
$R_c^{(x)}$	–	0.627 138 794 [21]	0.457 5(1)	–
$R_c^{(2)}$	–	0.480 701 867 [21]	0.332 0(2)	–
$R_c^{(3)}$	–	–	0.267 2(2)	–
d_F	1.875 01(5)	15/8 [39,40]	2.481 8(4)	2.481 6(1) [37] 2.481 9(4) [5]
d_{\min}	1.094 0(2)	1.095 5(10) [44]	1.259 36(12)	–
d_B	1.732 1(4)	1.730 4(3) [46]	2.167 3(15)	2.171(4) [45]

with zero. On this basis, we perform the fit with fixed $b_1 = 0$. The fitting results are shown in Table V.

After comparing various fits, we obtain the critical thermodynamic bond densities of various types, including the branch bonds $\rho_{b,0}(3D) = 0.176\,526\,5(1)$ and $\rho_{b,0}(2D) = 0.183\,250\,2(5)$, the junction bonds $\rho_{j,0}(3D) = 0.010\,298\,2(1)$ and $\rho_{j,0}(2D) = 0.023\,856\,2(2)$, as well as the nonbridge bonds $\rho_{n,0}(3D) = 0.051\,342\,35(10)$ and $\rho_{n,0}(2D) = 0.292\,893\,7(9)$. The nonbridge density in two dimensions is very consistent with the exact result $0.292\,893\,219$ [47,48]. Among all the occupied bonds, the fraction of the branch, junction, and nonbridge bonds are 74.12%, 4.32%, and 21.56% for the 3D Ising model, 36.65%, 4.77%, and 58.58% for the 2D Ising model, respectively. This suggests that as the spatial dimension d increases, the critical FK clusters become more and more dendritic.

V. SUMMARY AND DISCUSSION

In this work, we investigate the Ising model from the perspective of the geometric properties of the FK clusters. We find that the wrapping probabilities, a kind of topological quantities, suffer less from finite-size corrections near the critical point, and thus they provide a powerful tool for locating the critical point. This leads to a high-precision estimate for the 3D Ising model $K_c = 0.221\,654\,631(8)$, a competing result with the most recent one, $0.221\,654\,626(5)$ [5]. The probability distribution is observed to follow a single-

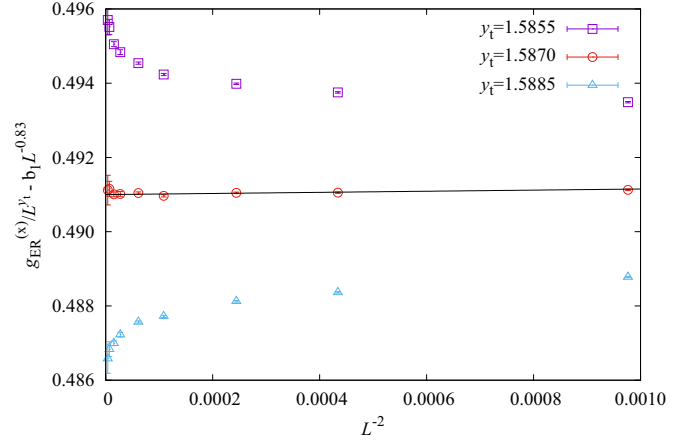


FIG. 8. Plot of $g_{ER}^{(x)}/L^{y_t} - b_1 L^{-0.83}$ vs L^{-2} for the 3D Ising model, using three different values of y_t . The value of b_1 is taken from Table VII.

variable function $P(C_1, L) dC_1 \equiv \tilde{P}(x) dx$, with $x \equiv C_1/L^{d_F}$. The scaling function $\tilde{P}(x)$ displays very rich behaviors within the scaling window $\Delta \equiv L^{y_t}(K - K_c)$, with a finite constant Δ , including a bimodal feature. We also study other quantities that characterize the geometric “compactness” of the critical FK clusters. In particular, we determine the shortest-path fractal dimension $d_{\min}(3D) = 1.259\,36(12)$ and $d_{\min}(2D) = 1.094\,0(2)$ from the graph distances and the backbone fractal dimension $d_B(3D) = 2.167\,3(15)$ and $d_B(2D) = 1.732\,1(4)$. A brief summary is given in Table VI.

The results for d_{\min} and d_B , together with the thermodynamic bond densities of various types, suggest that as the spatial dimension increases, the critical FK clusters become more and more dendritic. The FK representation of the Ising model provides much richer critical behaviors than the spin representation, some of which are not well understood yet. For instance, even in two dimensions, it remains an open question whether the shortest-path and backbone dimensions take some fractional numbers, and if so, what their values are. It also remains to understand the correction exponent -0.67 observed in the largest backbone cluster of the 2D Ising model.

The FK clusters display many geometric properties which are beyond the study of our work. For instance, in the frame-

TABLE VII. Fits of $g_{ER}^{(x)}$ for the 3D and 2D Ising models.

	L_{\min}	χ^2/DF	y_t	a_0	b_1	y_1	b_2
3D	12	6.5/8	1.586 7(3)	0.492 2(9)	-0.651(3)	-0.815(5)	–
	16	6.0/7	1.586 5(4)	0.493(2)	-0.648(6)	-0.811(7)	–
	24	4.8/6	1.587 0(6)	0.491(2)	-0.66(2)	-0.82(2)	–
	12	7.4/8	1.587 2(2)	0.490 4(4)	-0.672(3)	-0.83	0.09(3)
	16	5.0/7	1.587 0(2)	0.490 9(5)	-0.677(5)	-0.83	0.15(5)
	24	4.7/6	1.587 2(3)	0.490 6(9)	-0.673(10)	-0.83	0.1(2)
2D	6	7.5/12	0.999 8(8)	0.428(3)	-0.474(2)	-0.456(4)	–
	8	7.4/11	0.999 8(10)	0.428(4)	-0.474(2)	-0.456(6)	–
	12	7.0/10	1.000 5(15)	0.426(5)	-0.473(2)	-0.46(1)	–
	8	7.9/12	1.000 4(2)	0.425 9(3)	-0.472 6(8)	-0.46	–
	12	7.0/11	1.000 3(2)	0.426 2(5)	-0.473(1)	-0.46	–
	16	6.9/10	1.000 2(3)	0.426 3(6)	-0.474(2)	-0.46	–

TABLE VIII. Fits of the cluster number density ρ for the 3D and 2D Ising models.

	L_{\min}	χ^2/DF	ρ_0	a	y_i	b	y_1
3D	12	2.4/7	0.315 588 26(9)	-0.282 0(9)	1.587 5(7)	1.04(4)	-1.49(2)
	16	1.4/6	0.315 588 2(1)	-0.283(2)	1.587(1)	0.96(9)	-1.45(5)
	24	1.2/5	0.315 588 2(2)	-0.282(3)	1.587(2)	1.1(3)	-1.49(12)
	12	3.0/8	0.315 588 19(4)	-0.282 67(6)	1.587	1.01(2)	-1.470(7)
	16	1.4/7	0.315 588 21(5)	-0.282 73(7)	1.587	0.98(3)	-1.46(2)
	12	3.0/9	0.315 588 19(3)	-0.282 67(3)	1.587	1.009(2)	-1.47
	16	2.5/8	0.315 588 18(4)	-0.282 66(3)	1.587	1.007(3)	-1.47
	8	10.6/11	0.128 679 5(3)	-0.091 2(1)	1	0.974(3)	-1.002(2)
2D	12	10.6/10	0.128 679 4(4)	-0.091 2(2)	1	0.974(8)	-1.002(4)
	16	7.8/9	0.128 679 1(4)	-0.091 0(2)	1	0.993(14)	-1.009(6)
	8	11.2/12	0.128 679 6(2)	-0.091 29(4)	1	0.971 5(5)	-1
	12	10.8/11	0.128 679 6(3)	-0.091 27(5)	1	0.971 0(9)	-1
	16	10.3/10	0.128 679 6(3)	-0.091 30(6)	1	0.972(2)	-1

work of LCFT, a generalized class of two-point correlation functions can be defined on the basis of operators that insert N FK clusters with any given symmetry under the symmetric group \mathcal{S}_N , where $N \geq 1$ is an integer. These functions may exhibit rich behaviors under rotations, some of them can depend logarithmically on distance, and the corresponding critical exponents in three dimensions remain to be determined [9–11]. The intensive study of the conformal bootstrap method may also lead to significant progresses in percolation and the FK representation of the Potts model [6–8]. Our work might provide a solid numerical test ground for some fantastic theoretical developments in the future.

ACKNOWLEDGMENTS

This work was supported by the National Science Fund for Distinguished Young Scholars from the National Natural Science Foundation of China (NSFC) under Grant No. 11625522 (Y.J.D.), the National Science Fund for Young Scholars from the NSFC under Grant No. 11405039 (J.F.W.), the Fundamental Research Fund for the Central Universities from the Ministry of Finance and the Ministry of Education

of China under Grant No. J2014HGBZ0124 (J.F.W.), and the Start-up Fund from Anhui University under Grant No. J01006187 (H.H.).

APPENDIX: OTHER QUANTITIES

In addition to those in the main text, we have also considered several other quantities in the Monte Carlo simulations, including the following:

- The energy density \mathcal{E} and its square \mathcal{E}^2 , where \mathcal{E} is defined as $\mathcal{E} = \frac{1}{dL^d} \sum_{\langle ij \rangle} s_i s_j$.
- The number of clusters \mathcal{N}_c .
- The second cluster-size moments $\mathcal{S}_2 = \sum_k \mathcal{C}_k^2$, where the sum runs over all the clusters and \mathcal{C}_k denotes the size of the k th cluster.
- An observable $\mathcal{F} := \frac{1}{dL^d} \sum_{k=0}^{d-1} |\sum_{\mathbf{x}} s_{\mathbf{x}} \exp(i \frac{2\pi \mathbf{y}_k}{L})|^2$, which is the Fourier transform of the correlation function at the lowest nonzero momentum.

We measure the following quantities:

- The covariance of $\mathcal{R}^{(x)}$ and \mathcal{E} :

$$g_{ER}^{(x)} = \langle \mathcal{R}^{(x)} \mathcal{E} \rangle - \langle \mathcal{R}^{(x)} \rangle \langle \mathcal{E} \rangle, \quad (\text{A1})$$

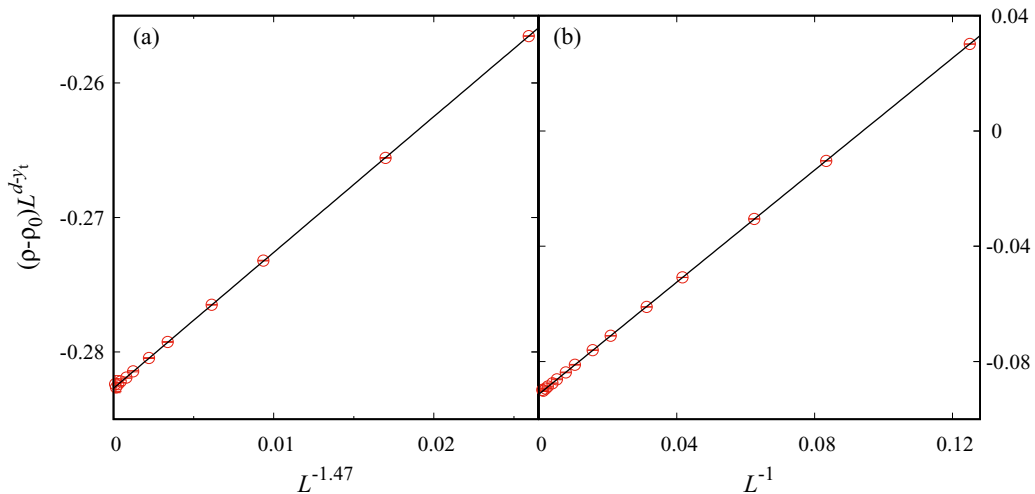


FIG. 9. Plots of the cluster number density $(\rho - \rho_0)L^{d\gamma_t}$ vs $L^{-1.47}$ for the 3D (a) Ising model and $(\rho - \rho_0)L$ vs L^{-1} for the 2D (b) Ising model at the critical temperature.

TABLE IX. Fits of C_e for the 3D and 2D Ising models.

	L_{\min}	χ^2/DF	α/ν	c_0	a_0	b_1	y_1	b_2
3D	8	7.1/8	0.169(1)	-3.61(7)	4.83(6)	-1.76(10)	-1.49(6)	-
	12	7.0/7	0.170(2)	-3.6(2)	4.8(1)	-1.7(3)	-1.4(2)	-
	16	4.5/6	0.174(5)	-3.3(4)	4.6(3)	-1.0(3)	-1.1(3)	-
	12	7.2/8	0.169 3(6)	-3.62(4)	4.84(3)	-1.77(4)	-1.5	-
	16	7.0/7	0.169 1(7)	-3.63(5)	4.85(4)	-1.74(8)	-1.5	-
	24	4.7/6	0.170(2)	-3.54(8)	4.78(6)	-2.0(2)	-1.5	-
	8	6.7/8	0.171(2)	-3.5(1)	4.73(8)	-0.24(8)	-0.83	-1.7(2)
	12	6.7/7	0.171(3)	-3.4(2)	4.7(2)	-0.3(2)	-0.83	-1.7(4)
2D	6	10.7/12	-	0.178(2)	0.6365(4)	-0.22(2)	-1	0.05(6)
	8	10.1/11	-	0.180(3)	0.6363(5)	-0.24(3)	-1	0.1(2)
	6	11.3/13	-	0.1772(9)	0.6367(2)	-0.211(4)	-1	-
	8	11.2/12	-	0.1774(1)	0.6367(3)	-0.212(6)	-1	-
	12	10.3/11	-	0.1785(2)	0.6365(4)	-0.22(1)	-1	-

which scales as $g_{ER}^{(x)} \sim L^{y_t}$ at K_c , with $y_t = 1/\nu$ the thermal exponent.

(b) The cluster number density $\rho = \langle \mathcal{N}_c \rangle / L^d$, whose leading scaling term is proportional to L^{y_t-d} .

(c) Specific heat $C_e = L^d(\langle \mathcal{E}^2 \rangle - \langle \mathcal{E} \rangle^2)$, which scales as $C_e \sim L^{2y_t-d} = L^{\alpha/\nu}$ at K_c .

(d) Susceptibility $\chi = \langle \mathcal{S}_2 \rangle / L^d$, which scales as $\chi \sim L^{2d_F-d} = L^{\gamma/\nu}$ at K_c .

(e) The second moment correlation length

$$\xi_{2\text{nd}} = \sqrt{\frac{\chi/F - 1}{4 \sin^2 \pi/L}}, \quad (\text{A2})$$

where $F = \langle \mathcal{F} \rangle$. At K_c , the ratio $\xi_{2\text{nd}}/L$ takes a nonzero universal value in the thermodynamic limit $L \rightarrow \infty$.

1. Estimating y_t

We estimate y_t by studying the covariance $g_{ER}^{(x)}$ for the 3D and 2D Ising models at the critical couplings $K = 0.221\,654\,63$ (3D) and $K_c = 0.440\,686\,79$ (2D), respectively. The MC data are fitted to Eq. (5) with y_A being replaced by y_t . We note that, in percolation case [25], a similar procedure for estimating y_t has been found preferable to methods, such as that employed in Ref. [49], in which y_t is estimated by studying how quantities behave in the neighborhood of the percolation threshold.

For the 3D Ising model, in the fit with $b_2 = 0$ fixed and y_1 free, we find $y_1 \approx -0.83$. We then perform the fit with $y_1 = -0.83$ and $y_2 = -2$ fixed. For the 2D Ising model, when leave $b_2 = 0$ fixed and y_1 free, we determine $y_1 \approx -0.46$. The fitting results are shown in Table VII.

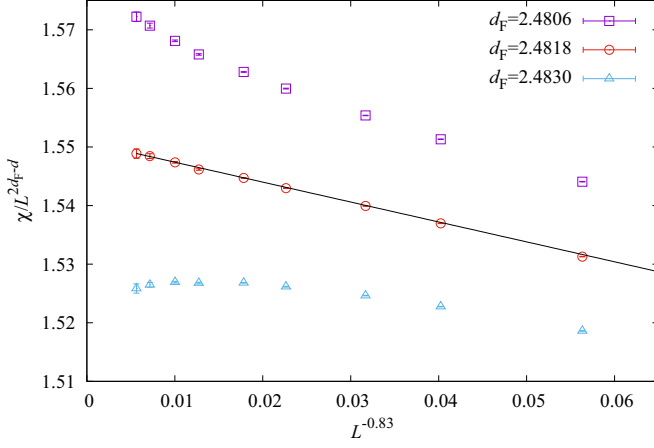
After comparing various fits, we estimate the thermal scaling exponent for the 3D and 2D Ising models as $y_t = 1.587\,0(5)$ (3D) and $1.000(1)$ (2D), respectively. In order to illustrate our estimate of y_t for the 3D Ising model, we plot $g_{ER}^{(x)}/L^{y_t} - b_1 L^{-0.83}$ versus L^{-2} using three different values of y_t : our estimate, as well as our estimate plus or minus three standard deviations, and show them in Fig. 8. Using the estimated value of y_t should produce a straight line for large L . In the figure, the data using $y_t = 1.585\,5$ and $y_t = 1.588\,5$ respectively bend upward and downward, suggesting that the true value of y_t does indeed lie within 3σ of our estimate. The data with $y_t = 1.587\,0$ appear to be consistent with an asymptotically straight line. For the 2D Ising model, our estimate of y_t is very consistent with the analytical result $y_t = 1$, as expected.

2. Cluster number density ρ

At $K = K_c$ and for $L \rightarrow \infty$, the FK cluster number density shall approach to a nonuniversal (model-dependent) constant ρ_0 . We fit the MC data of ρ for the 3D and 2D Ising models to Eq. (7). For the 3D Ising model, in the fit with y_t and

 TABLE X. Fits of χ for the 3D and 2D Ising models.

	L_{\min}	χ^2/DF	d_F	a_0	b_1	y_1	b_2
3D	8	5.6/8	2.481 77(16)	1.551(2)	-0.30(2)	-0.80(4)	-0.86(8)
	12	5.5/7	2.481 7(3)	1.552(3)	-0.29(5)	-0.78(8)	-0.9(2)
	8	6.2/9	2.481 88(3)	1.549 1(5)	-0.319(3)	-0.83	-0.79(2)
	12	5.9/8	2.481 86(5)	1.549 2(8)	-0.321(6)	-0.83	-0.77(5)
	16	4.8/7	2.481 82(7)	1.550(1)	-0.329(9)	-0.83	-0.7(1)
	8	12.8/11	1.875 00(2)	1.092 1(2)	-0.14(2)	-1.71(7)	-
2D	12	12.7/10	1.875 00(2)	1.092 0(2)	-0.16(6)	-1.8(2)	-
	16	10.4/10	1.875 007(10)	1.091 9(1)	-0.30(2)	-2	-
	24	10.4/9	1.875 007(13)	1.091 9(2)	-0.30(4)	-2	-
	32	7.0/8	1.875 02(2)	1.091 7(2)	-0.17(8)	-2	-


 FIG. 10. Plots of χ vs $L^{-0.83}$ at K_c for the 3D Ising model.

y_1 free, we observe that $y_t = 1.587(3)$ which is consistent with our estimated $y_t = 1.5870(5)$. On this basis, we further perform the fit with $y_t = 1.587$ fixed and y_1 free, and observe that the correction exponent $y_1 \approx -1.47$. To reduce one fitting parameter, we also try the fit with $y_t = 1.587$ and $y_1 = -1.47$ fixed. For the 2D Ising model, if letting $y_t = 1$ fixed and y_1 free, we observe that the correction exponent $y_1 \approx -1$. To reduce one fitting parameter, we then try the fit with $y_1 = -1$ fixed. The fitting results are shown in Table VIII. After comparing various fits, we estimate the critical cluster number densities as $\rho_0 = 0.315\,588\,2(2)$ (3D) and $0.128\,679\,6(6)$ (2D), respectively.

In Fig. 9 we plot $(\rho - \rho_0)L^{d-y_t}$ versus $L^{-1.47}$ (3D) and versus L^{-1} (2D). In both cases, for large system sizes the data points are arranged in a straight line, as expected.

3. Specific heat C_e

According to the scaling theory, specific heat at criticality scales as $C_e \sim L^{\alpha/\nu}$. In order to fit the MC data of C_e , the fitting ansatz (5) is reformulated by adding a constant term c_0 due to the existence of analytic background, leading to

$$A = c_0 + L^{y_A}(a_0 + b_1L^{y_1} + b_2L^{y_2}), \quad (\text{A3})$$

where the exponent y_A stands for α/ν . For the 3D Ising model, in the fit with $b_2 = 0$ fixed and y_1 free, we observe that $y_1 \approx -1.5$. To reduce one fitting parameter, we perform the subsequent fit with both $y_1 = -1.5$ and $b_2 = 0$ fixed. Besides, we also perform the fit with both $y_1 = -0.83$ and $y_2 = 2y_1 = -1.66$ fixed.

For the 2D Ising model, since $\alpha = 0$, the leading scaling term L^{y_A} changes to $\ln L$. We fit the MC data of C_e to the following equation [50,51]:

$$A = a_0 \ln L + c_0 + b_1L^{-1} + b_2L^{-2}. \quad (\text{A4})$$

In the fitting results b_2 is consistent with zero. On this basis, we perform the fit with $b_2 = 0$ fixed. The fitting results are reported in Table IX. For 2D Ising model, $a_0 = 0.6366(5)$ is consistent with the theoretical value $a_0 = 2/\pi$ [51].

4. Susceptibility χ

We fit the MC data of χ in both two and three dimensions to Eq. (5) with the exponent y_A replaced by $2d_F - d$. For the 3D Ising model, in the fit with $y_2 = -2$ fixed and y_1 free, we observe that $y_1 \approx -0.83$. To reduce one fitting parameter, in the subsequent fit we fix $y_1 = -0.83$ and $y_2 = -2$. For the 2D Ising model, when leave $b_2 = 0$ fixed and y_1 free, we determine $y_1 \approx -2$. On this basis, we perform the fit with $y_1 = -2$ and $b_2 = 0$ fixed. The fitting results are shown in Table X.

From these fits, we get the estimate $d_F = 2.481\,8(4)$ (3D) and $d_F = 1.875\,0(4)$ (2D), respectively. In Fig. 10 we plot χ/L^{2d_F-d} versus $L^{-0.83}$ using three different values of d_F for the 3D Ising model: our estimate, as well as our estimate plus or minus three standard deviations. As L increases, the data with $d_F = 2.4806$ and $d_F = 2.4830$ bend upward and downward, respectively, while the data with $d_F = 2.4818$ are consistent with an asymptotically straight line.

5. The second moment correlation length ξ_{2nd}

At $K = K_c$, the ratio ξ_{2nd}/L approaches a universal value $(\xi_{2nd}/L)_c$ in the thermodynamic limit $L \rightarrow \infty$. It means that the second moment correlation length scales as $\xi_{2nd} \sim L$. We fit the MC data of ξ_{2nd} for the 3D and 2D Ising models to Eq. (5) with $y_A = 1$ fixed and a_0 replaced by $(\xi_{2nd}/L)_c$. For the 3D Ising model, in the fit with $y_2 = -2$ fixed and y_1

 TABLE XI. Fits of ξ_{2nd} for the 3D and 2D Ising models.

	L_{\min}	χ^2/DF	$(\xi_{2nd}/L)_c$	b_1	y_1	b_2
3D	12	10/8	0.64321(9)	-0.026(4)	-0.72(6)	0.02(3)
	16	7.3/7	0.64310(10)	-0.037(10)	-0.83(9)	0.11(7)
	16	7.4/8	0.64310(3)	-0.0367(8)	-0.83	0.11(2)
	24	7.1/7	0.64309(4)	-0.036(1)	-0.83	0.09(5)
	32	6.9/6	0.64310(5)	-0.037(2)	-0.83	0.13(9)
2D	8	6.4/12	0.905 05(6)	0.46(2)	-1.54(2)	-
	12	6.3/11	0.905 06(7)	0.48(4)	-1.56(4)	-
	16	6.2/10	0.905 06(8)	0.47(7)	-1.55(6)	-
	8	6.5/13	0.905 06(4)	0.468(2)	-1.55	-
	12	6.3/12	0.905 05(4)	0.469(4)	-1.55	-
	16	6.2/11	0.905 06(5)	0.468(7)	-1.55	-

free, we observe that the correction exponent $y_1 \approx -0.83$. To reduce one fitting parameter, we further perform the fit with $y_1 = -0.83$ and $y_2 = -2$ fixed. For the 2D Ising model, if letting $b_2 = 0$ and y_1 free, we observe that the correction exponent $y_1 \approx -1.55$. To reduce one fitting parameter, we then try the fit with fixed $y_1 = -1.55$. The fitting results are shown in Table XI.

After comparing these fits, we determine the universal critical ratio as $(\xi_{2\text{nd}}/L)_c = 0.6431(1)$ (3D) and $0.90506(8)$ (2D), respectively. The current estimates for the 3D and 2D Ising models agree well with the previous reported value $(\xi_{2\text{nd}}/L)_c(3\text{D}) = 0.6431(1)$ [38] and the numerical integration result $(\xi_{2\text{nd}}/L)_c(2\text{D}) = 0.9050488292(4)$ [52] using conformal field theory, respectively.

-
- [1] E. Ising, *Z. Phys.* **31**, 253 (1925).
 [2] L. Onsager, *Phys. Rev.* **65**, 117 (1944).
 [3] R. J. Baxter, *Exactly Solved Models in Statistical Mechanics* (Academic Press, New York, 1982).
 [4] J. Kaupuzs, J. Rimšāns, and R. V. N. Melnik, *Ukr. J. Phys.* **56**, 845 (2011).
 [5] A. M. Ferrenberg, J. Xu, and D. P. Landau, *Phys. Rev. E* **97**, 043301 (2018).
 [6] S. El-Showk, M. F. Paulos, D. Poland, S. Rychkov, D. Simmons-Duffin, and A. Vichi, *Phys. Rev. D* **86**, 025022 (2012).
 [7] F. Kos, D. Poland, D. Simmons-Duffin, and A. Vichi, *J. High Energy Phys.* **08** (2016) 036.
 [8] A. LeClair and J. Squires, *J. Stat. Mech.* (2018) 123105.
 [9] R. Vasseur and J. L. Jacobsen, *Nucl. Phys. B* **880**, 435 (2014).
 [10] R. Couvreur, J. L. Jacobsen, and R. Vasseur, *J. Phys. A* **50**, 474001 (2017).
 [11] X. Tan, R. Couvreur, Y. Deng, and J. L. Jacobsen, *arXiv:1809.06650* (2018).
 [12] P. W. Kasteleyn and C. M. Fortuin, *J. Phys. Soc. Jpn. Suppl.* **26**, 11 (1969); C. M. Fortuin and P. W. Kasteleyn, *Physica (Amsterdam)* **57**, 536 (1972).
 [13] F. Y. Wu, *Rev. Mod. Phys.* **54**, 235 (1982).
 [14] J. L. Cardy, in *Phase Transitions and Critical Phenomena*, edited by C. Domb and J. L. Lebowitz, Vol. 11 (Academic Press, London, 1987), p. 55.
 [15] G. F. Lawler, O. Schramm, and W. Werner, *Math. Res. Lett.* **8**, 401 (2001).
 [16] R. H. Swendsen and J. S. Wang, *Phys. Rev. Lett.* **58**, 86 (1987).
 [17] R. G. Edwards and A. D. Sokal, *Phys. Rev. D* **38**, 2009 (1988).
 [18] L. Chayes and J. Machta, *Physica (Amsterdam)* **254**, 477 (1998).
 [19] H. T. Pinson, *J. Stat. Phys.* **75**, 1167 (1994).
 [20] L. P. Arguin, *J. Stat. Phys.* **109**, 301 (2002).
 [21] R. P. Langlands, C. Pichet, P. Pouliot, and Y. Saint-Aubin, *J. Stat. Phys.* **67**, 553 (1992).
 [22] See, e.g., J. P. Hovi and Amnon Aharony, *Phys. Rev. E* **53**, 235 (1996); L. N. Shchur and S. S. Kosyakov, *Int. J. Mod. Phys. C* **08**, 473 (1997); L. N. Shchur and T. Rostunov, *JETP Lett.* **76**, 475 (2002).
 [23] K. Binder, *Z. Phys. B* **43**, 119 (1981).
 [24] P. H. L. Martins and J. A. Plascak, *Phys. Rev. E* **67**, 046119 (2003).
 [25] J. Wang, Z. Zhou, W. Zhang, T. M. Garoni, and Y. Deng, *Phys. Rev. E* **87**, 052107 (2013).
 [26] X. Xu, J. Wang, J.-P. Lv, and Y. Deng, *Front. Phys.* **9**, 113 (2014).
 [27] H. Hu, H. W. J. Blöte, and Y. Deng, *J. Phys. A* **45**, 494006 (2012).
 [28] H. Hu and Y. Deng, *Nucl. Phys. B* **898**, 157 (2015).
 [29] J. L. Jacobsen and C. R. Scullard, *J. Phys. A* **45**, 494003 (2012).
 [30] J. L. Jacobsen, *J. Phys. A* **47**, 135001 (2014).
 [31] U. Wolff, *Phys. Rev. Lett.* **62**, 361 (1989).
 [32] X. Xu, J. Wang, Z. Zhou, T. M. Garoni, and Y. Deng, *Phys. Rev. E* **89**, 012120 (2014).
 [33] W. Huang, P. Hou, J. Wang, R. M. Ziff, and Y. Deng, *Phys. Rev. E* **97**, 022107 (2018).
 [34] H. J. Herrmann, D. C. Hong, and H. E. Stanley, *J. Phys. A* **17**, L261 (1984).
 [35] P. Grassberger, *Physica A (Amsterdam)* **262**, 251 (1999).
 [36] E. P. Mürger and M. A. Novotny, *Phys. Rev. B* **43**, 5773 (1991).
 [37] Y. Deng and H. W. J. Blöte, *Phys. Rev. E* **68**, 036125 (2003).
 [38] M. Hasenbusch, *Phys. Rev. B* **82**, 174433 (2010).
 [39] C. N. Yang, *Phys. Rev.* **85**, 808 (1952).
 [40] B. Nienhuis, in *Phase Transitions and Critical Phenomena*, edited by C. Domb and J. L. Lebowitz, Vol. 11 (Academic Press, London, 1987), p. 1.
 [41] C. Ruge and F. Wagner, *J. Stat. Phys.* **66**, 99 (1992).
 [42] C. Ruge, S. Dunkelmann, F. Wagner, and J. Wulf, *J. Stat. Phys.* **73**, 293 (1993).
 [43] M. D'Onorio de Meo, D. W. Heermann, and K. Binder, *J. Stat. Phys.* **60**, 585 (1990).
 [44] Y. Deng, W. Zhang, T. M. Garoni, A. D. Sokal, and A. Sportiello, *Phys. Rev. E* **81**, 020102(R) (2010).
 [45] Y. Deng and H. W. J. Blöte, *Phys. Rev. E* **70**, 046106 (2004).
 [46] Y. Deng, H. W. J. Blöte, and B. Nienhuis, *Phys. Rev. E* **69**, 026114 (2004).
 [47] E. M. Elci, M. Weigel, and N. G. Fytas, *Nucl. Phys. B* **903**, 19 (2016).
 [48] H. Hu, H. W. J. Blöte, R. M. Ziff, and Y. Deng, *Phys. Rev. E* **90**, 042106 (2014).
 [49] Y. Deng and H. W. J. Blöte, *Phys. Rev. E* **72**, 016126 (2005).
 [50] A. E. Ferdinand and M. E. Fisher, *Phys. Rev.* **185**, 832 (1969).
 [51] J. Salas, *J. Phys. A* **34**, 1311 (2001).
 [52] J. Salas and A. D. Sokal, *J. Stat. Phys.* **98**, 551 (2000).